Volume 9 | Number 11 | 21 March 2017 | Pages 3659–4036

Nanoscale

rsc.li/nanoscale

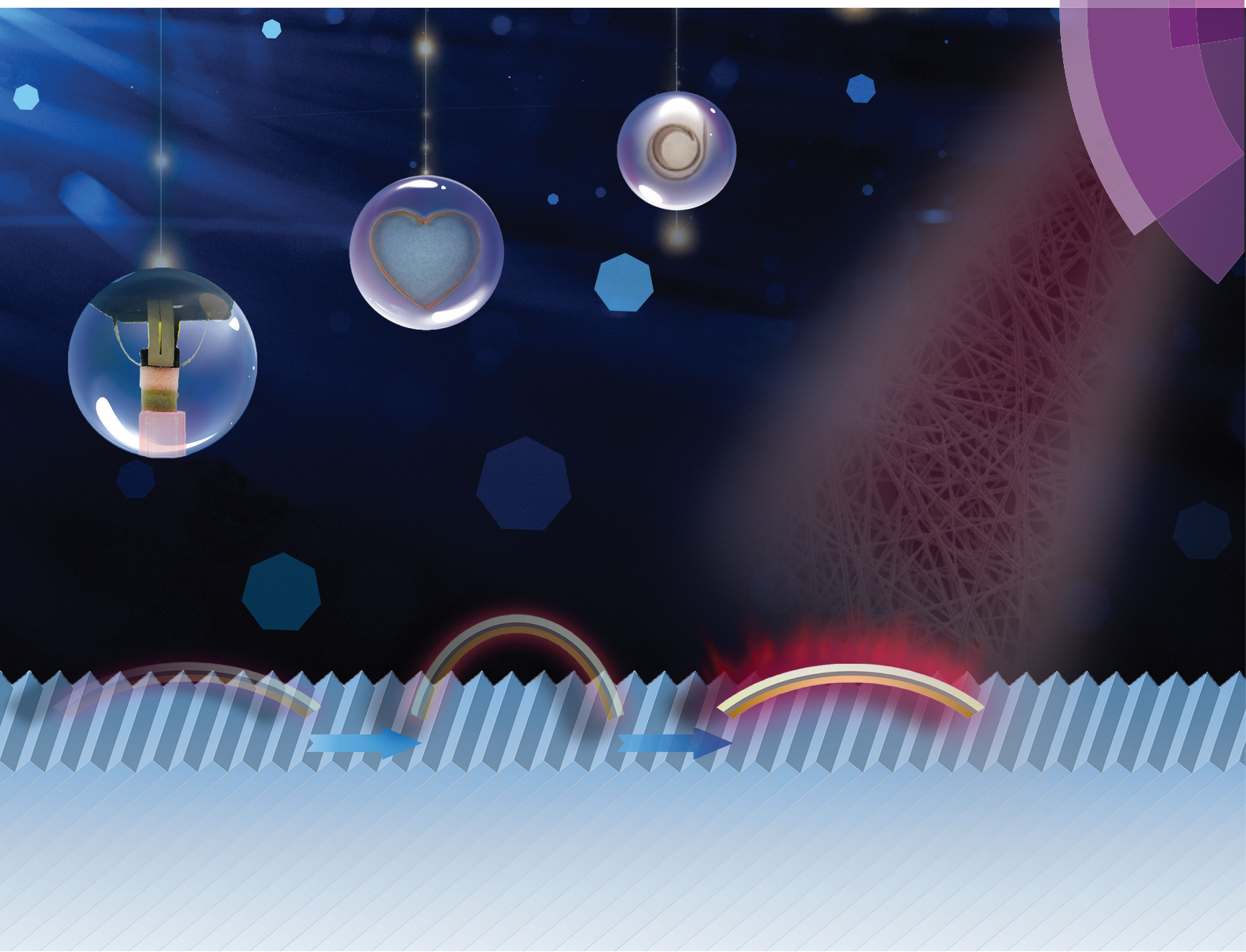

ISSN 2040-3372

ROYAL SOCIETY OF CHEMISTRY

PAPER
Yong Zhu *et al.*
Soft electrothermal actuators using silver nanowire heaters

NCNST

Nanoscale

PAPER

View Article Online
View Journal | View Issue

Cite this: *Nanoscale*, 2017, **9**, 3797

Soft electrothermal actuators using silver nanowire heaters†

Shanshan Yao, Jianxun Cui, Zheng Cui and Yong Zhu*

Received 29th November 2016,
Accepted 11th January 2017

DOI: 10.1039/c6nr09270e

rsc.li/nanoscale

Low-voltage and extremely flexible electrothermal bimorph actuators were fabricated in a simple, efficient and scalable process. The bimorph actuators were made of flexible silver nanowire (AgNW) based heaters, which exhibited a fast heating rate of 18 °C s^{-1} and stable heating performance with large bending. The actuators offered the largest bending angle (720°) or curvature (2.6 cm^{-1}) at a very low actuation voltage (0.2 V sq^{-1} or 4.5 V) among all types of bimorph actuators that have been reported to date. The actuators can be designed and fabricated in different configurations that can achieve complex patterns and shapes upon actuation. Two applications of this type of soft actuators were demonstrated towards biomimetic robotics – a crawling robot that can walk spontaneously on ratchet surfaces and a soft gripper that is capable of manipulating lightweight and delicate objects.

1. Introduction

Soft robots that can mimic biological systems with lifelike motions (*e.g.* walkers, swimmers, rollers, grippers, tentacles) have received much interest recently.[1,2] Compared with the conventional rigid counterparts that typically consist of heavy and complex components, soft robots, composed of flexible components with multiple degrees of freedom, can accomplish complex motions in a relatively simple way.[3] Besides, due to the remarkable flexibility, soft robots can better manipulate delicate objects, resist mechanical damage and adapt to the environment.[4] As a key part, soft actuators that respond to applied external stimuli such as light,[2,5] electric field,[6–8] magnetic field,[9,10] and pneumatic pressure[4,11] have been explored towards biomimetic applications.

Among the various types of stimuli, electric stimulus represents one of the simplest and most convenient ways. Electroactive polymers (EAPs), mainly ionic or field-activated polymers, have been widely used for actuation.[12–16] However, the ionic activation typically operates in an electrolyte environment and the field activation requires high voltage (>1 kV), which pose challenges for their practical applications.[17,18] Recently, another type of electromechanical actuators, electrothermal actuators, based on either thermal expansion of a single material[19] or difference in thermal expansion of two materials,[6,17,20–25] have drawn significant attention due to the simple operation, lightweight, low actuation voltage and being electrolyte-free.

Carbon nanotube (CNT)[6,17,19–21] and graphene[22–25] are commonly used in soft electrothermal actuators as the heater to introduce temperature change by joule heating. However, the relatively high electrical resistance of CNTs or graphene heaters increases the actuation voltage. For example, most of these electrothermal actuators are operated under tens of volts,[17,21,25] with very few exceptions.[6,20] The high voltage makes such actuators challenging for real applications in addition to causing safety concerns. It is important to develop flexible heaters with low electrical resistance in order to reduce the actuation voltage. In addition, for almost all the reported actuators (not limited to electrothermal actuators), the generated bending angle or curvature is relatively small (typically less than 1 cm^{-1} in curvature[2,17,20,25,26]), which may limit the realization of sophisticated and multiform motions. Therefore, electrolyte-free, low-voltage soft actuators that can achieve large bending deformation are highly desirable.

Here a silver nanowire (AgNW) based bimorph actuator offers the largest bending angle of 720° and a curvature of 2.6 cm^{-1} at a low actuation voltage of 0.2 V sq^{-1} (4.5 V) among all types of bimorph actuators that have been reported, to the best of our knowledge. The outstanding performances at an ultra-low voltage should be largely ascribed to the high

Department of Mechanical and Aerospace Engineering, North Carolina State University, Raleigh, NC 27695, USA. E-mail: yong_zhu@ncsu.edu

†Electronic supplementary information (ESI) available: Heating/cooling rate of AgNW/PDMS heaters, calibrated emissivity of AgNW/PDMS heaters, equations and calculation details on the bending angle and curvature of the bimorph actuators, a summary of the response time for electrothermal bimorph actuators, calculations of the response time of electrothermal bimorph actuators, a summary of the reported performance for bimorph actuators, calculation of the bending curvature using the length and displacement of the actuator, and stability of the PI/AgNW/PDMS actuator. Supplementary Movies: bending behavior of the PI/AgNW/PDMS actuator (S1), walker crawling on a flat ratchet surface (S2), walker crawling upstairs (S3), walker crawling downstairs (S4), gripper grab and collect (S5), and gripper pick and place (S6). See DOI: 10.1039/c6nr09270e

conductivity and mechanical robustness of the AgNW heater with large deformation, the significant difference in thermal expansion between PDMS and PI, and the excellent thermal stability of all the materials used. The heater and actuator are fabricated by a simple and low-cost process. Controllable and reconfigurable patterns with a large curvature can be realized by designing the actuators into different configurations. The utility of such soft actuators towards biomimetic soft robotics is demonstrated by a walking device that can crawl autonomously on a ratchet surface and a soft gripper that can manipulate lightweight and delicate objects. The reported bimorph actuators pushed the envelope of electrothermal actuators. It should be emphasized that the materials chosen, especially the AgNWs, play the key role to achieve the outstanding performances as reported. Note that the actuation voltage is related to the dimension of the heater, so in this paper the voltage is normalized to volt per square ($V_{sq} = V/(l/w)$, where V is the voltage, l and w are the length and width of the actuator, respectively) for the purpose of comparing with other actuators.

2. Results and discussion

2.1 Heating performance of the AgNW heater

Flexible heaters have attracted much attention for applications such as defogging windows, flexible displays, heating source of sensors, healthcare and personal thermal management.[27–29] A variety of materials such as CNTs,[30,31] graphene,[32] silver nanoparticles (AgNPs),[33] silicon nanoribbons[34] were explored as flexible heaters. Due to their large aspect ratio and high electrical conductivity, AgNWs are excellent conductive and flexible scaffolds to construct effective conducting networks[28,35,36] and have been used as flexible heaters, where AgNWs are typically deposited on top of the substrates and could be scratched or delaminated with repeated bending.[37,38]

To improve the mechanical robustness, in this work the AgNW network was embedded just below the surface of PDMS following a fabrication process reported previously[39–41] (Fig. 1a and b). The resulting AgNW/PDMS composite conductor was highly conductive, twistable, foldable and stretchable (Fig. 1c) and thus used as a highly flexible heater for the electrothermal bimorph actuator. The performances of the heater were first studied with respect to the applied voltage and the sheet resistance. Fig. 1d and e present the time-dependent temperature profiles of five heaters with different sheet resistances at a fixed voltage of 1.5 V (0.15 V sq^{-1}) and of a given heater (0.25 Ω sq^{-1}) at different voltages, respectively. The heater temperature increased rapidly after the heater was turned on and then increased until reaching a steady-state temperature (saturation temperature). When the heater was turned off, the temperature dropped quickly until room temperature. The saturation temperature increased monotonically with decreasing sheet resistance or increasing applied voltage. The input electrical power P is related to the voltage V and the resistance R by $P = V^2/R$. The saturation temperature of the heater can be determined by[27,42]

$$T_{\text{steady-state}} = \frac{V^2/R - Q_d}{Cm} + T_0 \quad (1)$$

where T_0 is the room temperature, C is the heat capacity, m is the mass, and Q_d is the total heat dissipated. The saturation temperature *vs.* the input power density (input power normalized by the heater area) can be fitted into a linear relationship with a slope of 216 °C cm^2 W^{-1} (Fig. 1f). For the heater with a sheet resistance of 0.25 Ω sq^{-1}, the temperature of the heater can reach around 160 °C at a low voltage of 0.2 V sq^{-1} (2 V). This is the lowest voltage required to generate such a high temperature, among all the reported flexible heaters (*e.g.* 50 °C

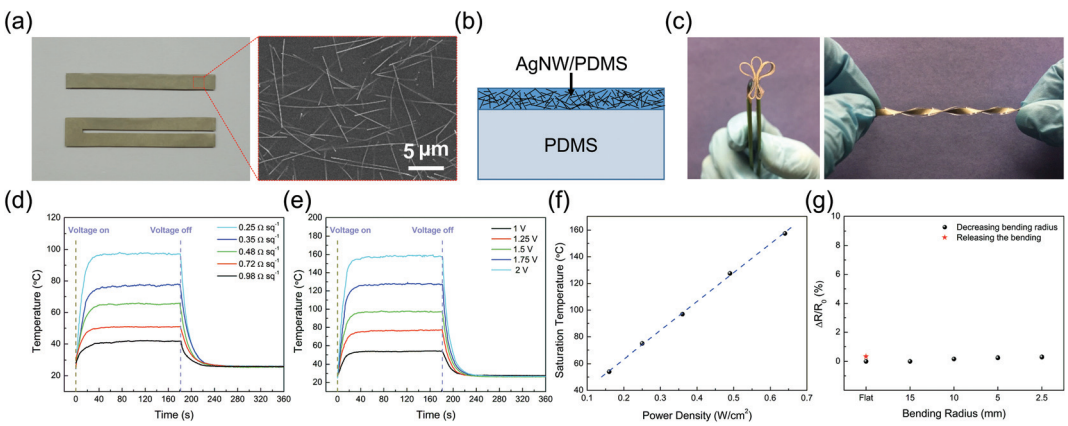

Fig. 1 Morphology and heating performance of the AgNW heater. (a) Photograph of the as-prepared AgNW/PDMS heaters and the SEM image showing the top surface of the heater. AgNWs were embedded just below the surface of PDMS. (b) Schematic showing the cross-section of the AgNW/PDMS heater. (c) Photographs of the AgNW/PDMS heaters being folded and twisted. (d) Time-dependent temperature profiles for heaters with different sheet resistances at a constant voltage of 1.5 V. (e) Time-dependent temperature profiles when the heater (sheet resistance of 0.25 Ω sq^{-1}) was subjected to different voltages. The voltage was on for 180 s. (f) Saturation temperature of the heater as a function of the input power density for the heater with a sheet resistance of 0.25 Ω sq^{-1}. The blue dashed line shows a linear fitting of the experimental data. (g) Relative resistance change of a AgNW/PDMS heater as a function of bending radius.

at 7 V for AgNW/PEN,[38] ~160 °C at 50 V or 50 V sq^{-1} for graphene oxide/PI,[32] ~105 °C at 7 V or 4.67 V sq^{-1} for AgNW/PET[43] and ~95 °C at 12 V or 12 V sq^{-1}for CNT/PET[31]).

The rising time to the saturation temperature was ~30 s and the decay time back to room temperature was less than 60 s. The response time was faster than the reported heaters using AgNW/PEN,[38] AgNW/PET,[44] graphene/PET,[45] and comparable to those using CNT/PET,[31] AgNW-CNT/PET[46] and the AgNW/copolymer.[47] The heating and cooling rates of the AgNW/PDMS heater followed the same trend with the saturation temperature – the lower the sheet resistance or the higher the voltage, the higher the rates (Fig. S1 in the ESI†). The maximum heating rate of 18 °C s^{-1} and cooling rate of −20 °C s^{-1} were obtained for the heater with a sheet resistance of 0.25 Ω sq^{-1} at an applied voltage of 2 V, which is much higher than the heaters based on AgNW/PEN (2 °C s^{-1}),[38] CNT/glass (2 °C s^{-1})[48] and comparable to those based on graphene/PI (16 °C s^{-1})[32] and AgNW/PTBA composite (17 °C s^{-1}).[49]

Since the heater is expected to experience large bending during the bimorph actuation, stable heater performance at a large curvature (or a small bending radius) is required. The heater was bent to different radii and the resistance changes were recorded, as given in Fig. 1g. The resistance change was found to be less than 0.33% even with a very small bending radius of 2.5 mm, corresponding to a bending strain of ~4% (considering thicknesses of ~200 μm). The results demonstrated that the flexible AgNW/PDMS heater can provide high temperature at a very low voltage and stable performance with large bending, making it a promising candidate for electrothermal actuators.

2.2 Characterization of the PI/AgNW/PDMS bimorph actuator

An electrothermal bimorph actuator is based on the strain mismatch in two materials with different coefficients of thermal expansion, as schematically illustrated in Fig. 2a. A good electrothermal bimorph actuator requires the following: (1) the heater, placed between or on one side of the two materials, should offer good and stable heating performance during bending. Large bending strain can be involved if the heater is not placed in the neutral plane. (2) The two materials should have a large difference in the coefficient of thermal expansion. (3) The two materials themselves should be stable over a wide temperature range. (4) Low voltage actuation is desirable.

A bimorph actuator was fabricated by simply bonding the AgNW/PDMS heater to PI tape. Note that one side of the AgNW/PDMS heater (thickness of ~200 μm) was pure PDMS and the other side was the conductive composite of AgNW/PDMS (see Fig. 1b). The PI tape was 12.5 μm (0.5 mil) in thickness. PDMS and PI were selected as the two active materials owing to their large difference in the coefficient of thermal expansion (α_{PDMS} = 310 × 10^{-6} K^{-1}, α_{PI} = 20 × 10^{-6} K^{-1}) and their stability to operate at a high temperature. The PI/AgNW/PDMS sandwich can be cut into the desired shapes and dimensions. For example, strip actuators were used for the walkers and U-shaped actuators were used for the actuator characterization and the grippers. This simple "tape and cut" process for making the soft actuators can be readily extended to mass fabrication.

Upon applying a DC voltage of 4.5 V, the bimorph actuator reached the maximum curvature in around 40 s and maintained the curvature with the voltage on. Upon turning off the

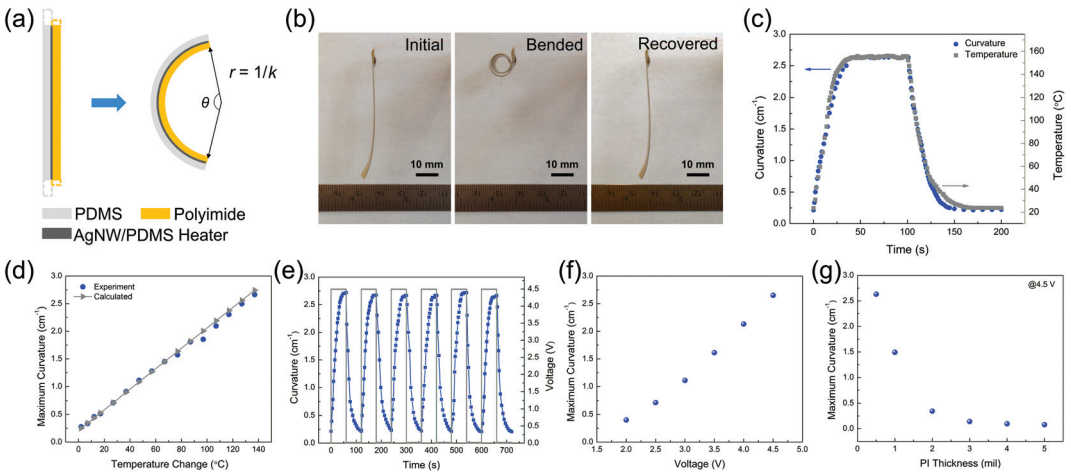

Fig. 2 Bending performance of the PI/AgNW/PDMS bimorph actuator. (a) Schematic of the electrothermal bimorph actuation mechanism. *k*: bending curvature; *r*: radius of curvature. (b) The initial state, the bent state with the maximum curvature and the recovered state of the U-shaped actuator. One end of the actuator is fixed and the other end can bend freely and reversibly under an applied DC voltage of 4.5 V. The corresponding movie is provided in Movie S1 in the ESI.† (c) Curvature and temperature of the actuator as functions of time. (d) Comparison of the calculation and the experimental results on the generated curvature *versus* the temperature change. (e) Cyclic actuation of the PI/AgNW/PDMS actuator when subjected to six cycles of voltage pulses (4.5 V amplitude, 60 s on and 60 s off). (f) Curvature as a function of applied DC voltage. (g) Curvature as a function of PI thickness under an applied voltage of 4.5 V DC.

voltage, the tip of the actuator completely restored the initial position within 60 s when the temperature reached room temperature, as shown in Fig. 2b, c and Movie S1.† Besides many advantages such as simple fabrication and operation, lightweight, low voltage and large bending angle, it is known that electrothermal actuators possess relatively slow response speed. However, our actuator outperforms most electrothermal actuators in terms of response speed for the same bending curvature (Table S1†). As discussed in the ESI† (section 4), a reduced response time of electrothermal actuators can be achieved by decreasing the thickness, decreasing the specific heat capacity, decreasing the material density, decreasing the surface area, or by increasing the input power (V^2/R), increasing the difference in the coefficient of thermal expansion, or by optimizing the total heat transfer coefficient and the ratios of Young's modulus and thickness of the two layers. For our actuators, the faster response speed can be attributed to the decreased thickness of the heater due to the high conductivity of the AgNWs, the large difference in the coefficient of thermal expansion between PI and PDMS and the optimized geometry of the actuator. Using longer AgNWs can help form a more effective conductive network and thus decrease the amount/mass of AgNWs needed to achieve the same conductivity,[36,50] which can further reduce the time constant and shorten the response time (eqn (6) in the ESI†).

A maximum bending angle of 720° and curvature of 2.6 cm^{-1} were achieved with an input power density of 5.11 mW mm^{-2} or 24.06 mW mm^{-3}. The bending angle and curvature realized in such a low voltage (0.2 V sq^{-1}) are significantly higher than almost all the reported bimorph actuators with any actuation method including electrothermal, photothermal or electrochemical actuators (see Fig. 3 and Table S2 in the ESI† for detailed comparisons). With the comparable input power density, the generated bending curvature is much larger. The typical bending curvature for an electrothermal bimorph actuator is less than 1 cm^{-1}.[17,20,21,25] Zeng and coworkers demonstrated CNT based actuators which exhibited a bending curvature of 0.29 cm^{-1} under a voltage of 7 V (1.17 V sq^{-1}) and input power density of 25 mW mm^{-3}. Chen and coworkers reported a large bending curvature of 1.2 cm^{-1} under a voltage of 10 V (0.56 V sq^{-1}).[22] Fan and coworkers have recently improved the bending angle to 389° with a curvature of 1.03 cm^{-1} under a voltage of 5 V (1.29 V sq^{-1}) and input power density of 31 mW mm^{-3}.[6] In addition to the optimized configuration of the bimorph actuator, the excellent and reversible bending behavior achieved here can be largely attributed to the stable performance of the AgNW/PDMS heater with large deformation, the significant difference in thermal expansion between PDMS and PI and excellent stability of all the materials used at high temperatures. Besides the large bending curvature, the actuation voltage was much smaller compared to other electrothermal actuators.[17,20,21,25]

Fig. 2c shows the bending curvature of the actuator and the corresponding temperature that was acquired by an infrared camera as functions of time. The average temperature obtained from the two surfaces of PDMS and PI was used here; no obvious difference in the temperatures was measured from the two surfaces anyway. The change in the curvature nearly

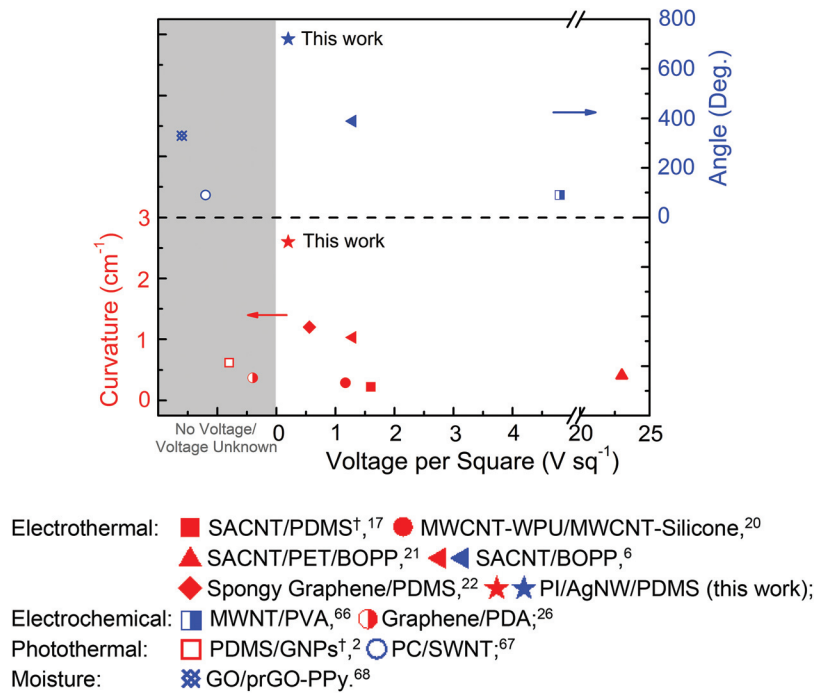

Fig. 3 Summary of the reported bending angle and curvature for bimorph actuators. For those marked with †, the curvature was not directly reported but calculated here using the given length and displacement of the actuator (see the ESI† for details).

followed the temperature change. The measurements agreed well with the calculation results, predicting that the curvature has a linear relationship with the temperature change, as indicated in Fig. 2d. More details on the calculation are provided in the ESI.† Six cycles of square voltage pulses with an amplitude of 4.5 V, a period of 120 s and a duty ratio of 1 : 1 were applied to examine the transient response of the actuator, as shown in Fig. 2e. The actuator exhibited immediate response and was totally reversible. Fig. 2f and g show the maximum bending curvature as a function of the applied voltage and the thickness of the PI layer, respectively, with the PDMS thickness unchanged.

Failure in the AgNW heater and actuators may occur under high electrical current and/or high temperature. Electromigration can lead to electrical stress.[51] Electromigration in AgNWs has been observed at a current density of 10^7–10^8 A cm^{-2}.[52,53] The maximum cross-sectional current density for the AgNW/PDMS heater in our case is much lower (~300 A cm^{-2}). The current density in an individual nanowire is unknown considering the network structure with multiple AgNW junctions. Yang *et al.*[54] found that the electromigration in AgNW networks (transparent electrodes with low AgNW density) can enhance the ripening of AgNW junctions, leading to reduced resistance. In our case, we did not observe obvious decrease in resistance under the applied electrical current, which might be because the AgNW density used here is significantly high (*i.e.* much lower current density in each individual nanowire), and the heater was subjected to thermal annealing at 150 °C before applying voltage (*i.e.* the nanowire junctions have already been ripened during thermal annealing). Rayleigh instability was observed in AgNWs and the onset temperature is related to the dimension of the AgNWs.[55,56] Bellet *et al.*[56] reported the onset of morphological instability starting from 300 °C for the AgNWs with a length of ~37.3 μm and diameter of ~105 nm (similar to our case). In our case the maximum operating temperature is 160 °C, so the Rayleigh instability should not be a significant problem. In order to test the stability of the heater and the actuators, we performed cyclic testing with square voltage pulses with an amplitude of 4.5 V for 500 cycles. No significant degradation in temperature and the bending curvature of the PI/AgNW/PDMS actuators were observed after 500 cycles (Fig. S4 in the ESI†), indicating good reliability and stability.

2.3 Designing the actuators to achieve various patterns

Due to the capability of large deformation and simple fabrication process, the reported actuator can be easily configured to achieve various desired patterns upon actuation. The PI/AgNW/PDMS composite bends to the PI side, while PDMS/AgNW or symmetric PI/PDMS/AgNW/PI results in negligible bending curvature. As shown in Fig. 2f, as the thickness of the PI tape increases, the bending angle decreases. Increasing the width of the AgNW/PDMS heater with the other parameters remaining constant decreases the power density, leading to a reduced bending angle. Therefore, the bending position can be controlled by where the PI tape is attached, while the bending curvature controlled by the thickness of PI and the width of the AgNW heater. As demonstrations, "NCSU" and "heart" patterns were obtained as illustrated in Fig. 4. Note, here the maximum curvature in letter "N" (marked by dashed circle) was ~1.8 cm^{-1}. Such patterns with a large curvature can only be achieved with actuators that can generate large deformations, as demonstrated in this work. More complex structures can be achieved by designing the actuator into different configurations.

2.4 Application of the soft actuator as a self walker

Self walking and grabbing objects are among the basic motions of robots and are often achieved in industrial robots using electric motors and/or hydraulics with complex and rigid components.[57,58] We developed prototypes of walkers that can crawl with a worm-like motion and soft grippers that can handle lightweight objects in a simple way without any

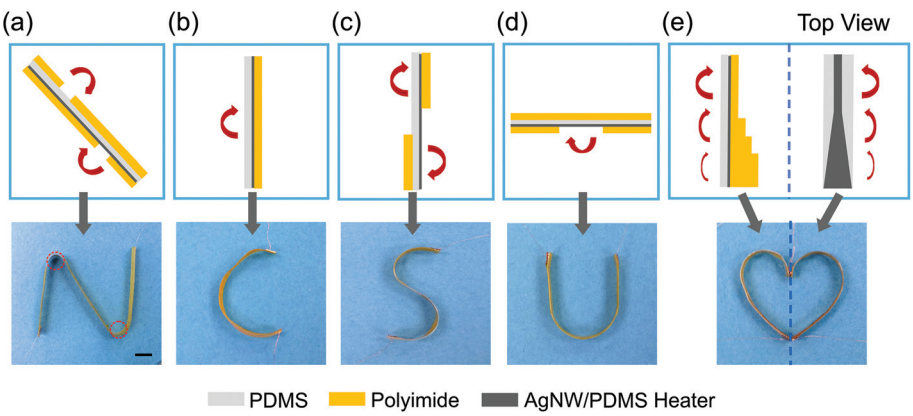

Fig. 4 Manipulation of the actuator configurations to achieve various bending patterns. (a)–(d) NCSU patterns by changing the position of PI tape. The marked areas by dotted circles show the maximum curvature. (e) The "heart" shape was intentionally made of two separate parts to indicate two methods, that each can be used to make half of a heart shape. The left part was achieved by gradually changing the thickness of PI tape (left) and the right part by gradually changing the width of the AgNW heater and thus the current density (right). Note that for the right part, only the top view from the PDMS side is shown and PI has the identical dimensions as PDMS. Scale bar: 10 mm.

complex components. The self walker, composed of a strip of PI/AgNW/PDMS actuator, was actuated with periodic electrical stimuli. The two legs moved closer when the voltage was applied and moved apart when the voltage was turned off. A ratchet mechanism[59,60] with an asymmetrical surface structure was employed to promote one-directional walking motion (Fig. 5a). During the bending step, the rear leg slid forward while the front leg was prevented from sliding backwards. Similarly during the extending step, the front leg slid forward with the rear leg constrained by the ratchet surface. As a result, the repeated bending and extension motions of the two legs can be converted into a forward motion.

The bending and extension motions right after turning on or off the voltage are the most efficient (*i.e.* with the highest speed). Hence to increase the walking speed, a voltage cycle with a relatively short period was applied. In addition, the bending arc of the walker should be gentle (*i.e.* with a small curvature) to facilitate the sliding of the front leg on the substrate, therefore a relatively low voltage was preferred. Fig. 5c–e shows the successive profiles of the walkers crawling on a flat ratchet surface, upstairs and downstairs. In each panel, the first three images represent one bending-extension cycle and the last image shows the position of the walker after three consecutive cycles. Due to the difference in the stair angle and the

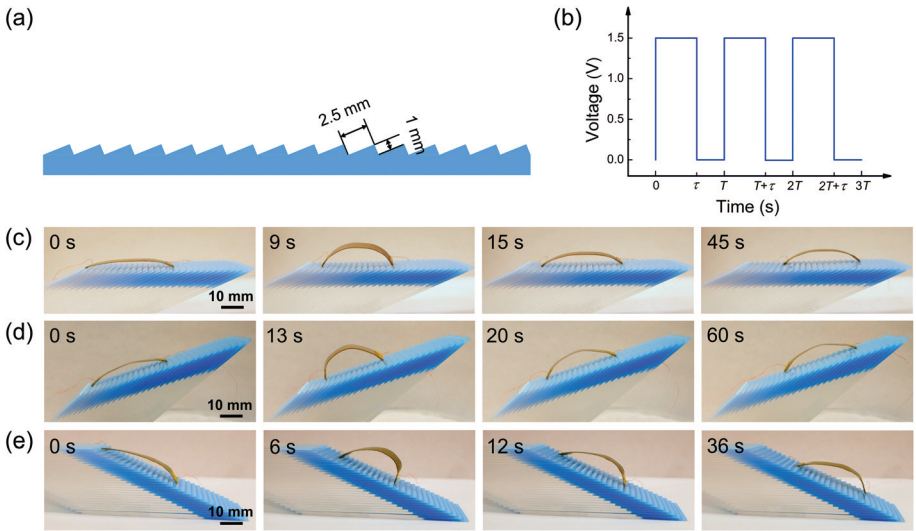

Fig. 5 Application of the soft actuator as a self walker. (a) Schematic of the ratchet surface prepared by stacking several glass slides with stair length (the distance between adjacent ratchet steps) of 2.5 mm and height of 1 mm. (b) To realize self-walking, periodic voltage pulse with the amplitude of 1.5 V was applied. τ indicates the voltage-on time and T indicates the period of the pulse. Consecutively captured images showing the walker crawling on a flat ratchet surface (c), upstairs (d) and downstairs (e) when the voltage is periodically turned on and off. The first three images in each panel shows one bending-extension cycle and the last image shows the position of the walker after three cycles. The corresponding movies are provided in Movie S2–4 in the ESI.†

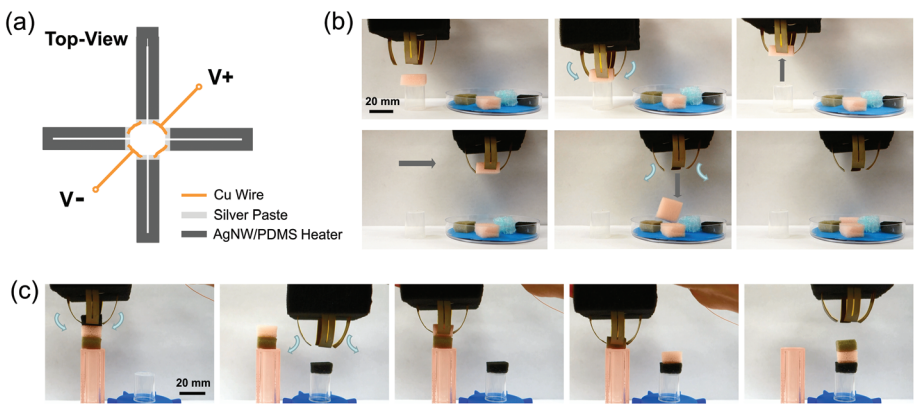

Fig. 6 Application of the soft actuators as a four-finger soft gripper. (a) Top-view schematic illustration showing the electrical connection of the four actuators. The dimensions are not drawn to scale. (b) Consecutively captured images showing the process of grabbing and collecting an object: approaching, grasping, lifting, moving and releasing. (c) Consecutively captured images showing the process of grabbing and placing three objects sequentially. The corresponding movies are provided in Movie S5–6 in the ESI.†

resulting friction from the substrate, the walking time for a flat ratchet surface, upstairs and downstairs was approximately 15 s, 20 s and 12 s per cycle, with the walking speeds of 25, 18 and 31 mm min^{-1}, respectively. The walking speed was larger than the self-walking gel using a ratchet mechanism (170 μm min^{-1})[61] and graphene-based photothermal walker with asymmetric friction to the substrate (3.8 mm min^{-1}).[62] The self-walking actuator demonstrated here can benefit the development of biomimetic robots that enable autonomous motions.

2.5 Application of the soft actuators as a four-finger soft gripper

Owing to the large deformation without the need for complex components and the gentle interaction with the objects, the soft actuator has been explored as a soft gripper to handle delicate objects.[3,57] A four-finger soft gripper was designed and fabricated to mimic humanoid motions. Each finger (a PI/AgNW/PDMS actuator) was patterned into U-shape to facilitate the connection to the power supply, as illustrated in Fig. 6a. Applying a voltage moved the four fingers closer as a result of the bending of the actuators, and turning off the voltage moved them apart, imitating the grabbing and releasing process of a human hand. Fig. 6b and c show how the gripper manipulated delicate objects (PU foam blocks) in "grab and collect" and "pick and place" motions. As demonstrated, the PI/AgNW/PDMS actuator can realize humanoid hand motions without any additional mechanical components and can be used as a robot "hand" to gently grab and transport fragile objects that cannot be handled with the conventional rigid robots. Increase in the output force (or equivalently the weight of the object that can be picked up by the actuator) can be achieved by reducing the length or increasing the width of the actuators, or by increasing the thickness, the Young's modulus and the difference in the coefficient of the thermal expansion of the two layers, or by increasing the temperature/input power.[63,64]

3. Conclusions

A novel soft electrothermal bimorph actuator was reported in this paper, where a highly conductive and flexible AgNW/PDMS conductor was employed as the flexible, efficient, and fast-responding heater. Due to the low sheet resistance, the heater can generate a high temperature of ~160 °C in 30 s with the maximum heating rate of 18 °C s^{-1} at a very low voltage of 0.2 V sq^{-1} (2 V). The heater performance was well-maintained with small bending radii. The reported actuator can achieve a very large bending angle of 720° or a curvature of 2.6 cm^{-1} under a low driven voltage of 0.2 V sq^{-1} (4.5 V). The outstanding performances are attributed to the high conductivity and good flexibility of the AgNW heater, the large mismatch in thermal expansion of PDMS and PI, and the excellent thermal stability of all materials used. Complex structures with a large curvature can be achieved by designing the actuator into different configurations. The potential applications of this soft actuator in soft robotics were demonstrated as self walkers and soft grippers. The fabrication process for the reported soft heater and actuator is simple and scalable. Realization of such high-performance soft actuators through simple design and fabrication, together with soft electronics and sensors,[65] represents a promising step towards soft robotics and soft machines.

4. Experimental section

4.1 Fabrication of AgNW/PDMS heaters and electrothermal bimorph actuators

AgNWs in ethanol (ACS Material) with an average diameter of 90 nm and length of 20–30 μm were shaken for 5 minutes before use to disperse the nanowires in the solution. The AgNW solution was drop-casted inside the grooves defined by a mask on a Si substrate; at the same time, the solution was heated by a hot plate at 50 °C to evaporate the solvent. After removing the mask, the patterned AgNWs were thermally annealed at 150 °C for 20 min. Then liquid PDMS with a weight ratio of 10 : 1 was spin-coated onto the AgNW film, degassed and subsequently thermally cured at 100 °C for 1 hour. Finally, the heater (AgNW/PDMS film) with the patterned AgNWs embedded below the surface of PDMS was peeled off the Si substrate. Multiple heaters can be fabricated in the same batch. Cu wires were attached to the two ends of the heaters by silver epoxy (MG Chemicals) for connection to the power supply. To assemble the bimorph actuator, commercial polyimide (PI) tapes (Kapton, Dupont) with different thicknesses were used as received. PI was attached onto the conductive side of the AgNW/PDMS heater and cut into the same dimension as the AgNW/PDMS heater. The integrated PI/AgNW/PDMS composite was then used as the bimorph actuator.

4.2 Characterization of AgNW/PDMS heaters and electrothermal bimorph actuators

The voltage was supplied to the heaters by a power supply (Agilent 6631C) and the resulting bending angles of the bimorph actuator were recorded by using a digital camera. The temperatures of the AgNW/PDMS heaters and the bimorph actuators were measured in real time using a non-contact infrared camera (FLIR A655SC) placed right over the heaters or actuators. The emissivity of materials was calibrated using black electrical tape over a temperature range of RT to 200 °C.

4.3 Fabrication of the four-finger gripper

Four U-shaped actuators were fabricated using the process mentioned above. A PU foam was used as a holder to fix the actuators and the interconnects. The fixed ends of the four actuators and their interconnects were embedded into the foam through pre-cut holes in the foam while the other ends of the actuators could bend freely.

Acknowledgements

The authors would like to acknowledge support by the National Science Foundation (NSF) through the ASSIST Engineering Research Center at NC State (EEC-1160483) and EFRI-1240438.

Notes and references

1 S. W. Kwok, S. A. Morin, B. Mosadegh, J. H. So, R. F. Shepherd, R. V. Martinez, B. Smith, F. C. Simeone, A. A. Stokes and G. M. Whitesides, *Adv. Funct. Mater.*, 2014, **24**, 2180–2187.
2 W. Jiang, D. Niu, H. Liu, C. Wang, T. Zhao, L. Yin, Y. Shi, B. Chen, Y. Ding and B. Lu, *Adv. Funct. Mater.*, 2014, **24**, 7598–7604.
3 R. V. Martinez, J. L. Branch, C. R. Fish, L. Jin, R. F. Shepherd, R. Nunes, Z. Suo and G. M. Whitesides, *Adv. Mater.*, 2013, **25**, 205–212.
4 R. V. Martinez, A. C. Glavan, C. Keplinger, A. I. Oyetibo and G. M. Whitesides, *Adv. Funct. Mater.*, 2014, **24**, 3003–3010.
5 Y. Hu, G. Wu, T. Lan, J. Zhao, Y. Liu and W. Chen, *Adv. Mater.*, 2015, **27**, 7867–7873.
6 L. Chen, M. Weng, Z. Zhou, Y. Zhou, L. Zhang, J. Li, Z. Huang, W. Zhang, C. Liu and S. Fan, *ACS Nano*, 2015, **9**, 12189–12196.
7 R. H. Baughman, C. Cui, A. A. Zakhidov, Z. Iqbal, J. N. Barisci, G. M. Spinks, G. G. Wallace, A. Mazzoldi, D. De Rossi, A. G. Rinzler, O. Jaschinski, S. Roth and M. Kertesz, *Science*, 1999, **284**, 1340–1344.
8 X. Zhao and Z. Suo, *Phys. Rev. Lett.*, 2010, **104**, 178302.
9 T. Kimura, Y. Umehara and F. Kimura, *Soft Matter*, 2012, **8**, 6206–6209.
10 S. R. Mishra, M. D. Dickey, O. D. Velev and J. B. Tracy, *Nanoscale*, 2016, **8**, 1309–1313.
11 B. Mosadegh, P. Polygerinos, C. Keplinger, S. Wennstedt, R. F. Shepherd, U. Gupta, J. Shim, K. Bertoldi, C. J. Walsh and G. M. Whitesides, *Adv. Funct. Mater.*, 2014, **24**, 2163–2170.
12 M. Bozlar, C. Punckt, S. Korkut, J. Zhu, C. C. Foo, Z. Suo and I. A. Aksay, *Appl. Phys. Lett.*, 2012, **101**, 091907.
13 T. Mirfakhrai, J. D. Madden and R. H. Baughman, *Mater. Today*, 2007, **10**, 30–38.
14 R. Pelrine, R. Kornbluh, Q. Pei and J. Joseph, *Science*, 2000, **287**, 836–839.
15 M. Kotal, J. Kim, K. J. Kim and I. K. Oh, *Adv. Mater.*, 2016, **28**, 1610–1615.
16 J. H. Choi, J. Ahn, J. B. Kim, Y. C. Kim, J. Y. Lee and I. K. Oh, *Small*, 2016, **12**, 1840–1846.
17 L. Chen, C. Liu, K. Liu, C. Meng, C. Hu, J. Wang and S. Fan, *ACS Nano*, 2011, **5**, 1588–1593.
18 Y. Bar-Cohen and Q. Zhang, *MRS Bull.*, 2008, **33**, 173–181.
19 Y. Hu, W. Chen, L. Lu, J. Liu and C. Chang, *ACS Nano*, 2010, **4**, 3498–3502.
20 Z. Zeng, H. Jin, L. Zhang, H. Zhang, Z. Chen, F. Gao and Z. Zhang, *Carbon*, 2015, **84**, 327–334.
21 L. Chen, M. Weng, W. Zhang, Z. Zhou, Y. Zhou, D. Xia, J. Li, Z. Huang, C. Liu and S. Fan, *Nanoscale*, 2016, **8**, 6877–6883.
22 Y. Hu, T. Lan, G. Wu, Z. Zhu and W. Chen, *Nanoscale*, 2014, **6**, 12703–12709.
23 P. Xiao, N. Yi, T. Zhang, Y. Huang, H. Chang, Y. Yang, Y. Zhou and Y. Chen, *Adv. Sci.*, 2016, **3**, 1500438.
24 S.-E. Zhu, R. Shabani, J. Rho, Y. Kim, B. H. Hong, J.-H. Ahn and H. J. Cho, *Nano Lett.*, 2011, **11**, 977–981.
25 H. Bi, K. Yin, X. Xie, Y. Zhou, S. Wan, F. Banhart and L. Sun, *Nanoscale*, 2013, **5**, 9123–9128.
26 J. Liang, L. Huang, N. Li, Y. Huang, Y. Wu, S. Fang, J. Oh, M. Kozlov, Y. Ma, F. Li, R. Baughman and Y. Chen, *ACS Nano*, 2012, **6**, 4508–4519.
27 Q. Huang, W. Shen, X. Fang, G. Chen, J. Guo, W. Xu, R. Tan and W. Song, *RSC Adv.*, 2015, **5**, 45836–45842.
28 S. Ji, W. He, K. Wang, Y. Ran and C. Ye, *Small*, 2014, **10**, 4951–4960.
29 D. H. Kim, S. Wang, H. Keum, R. Ghaffari, Y. S. Kim, H. Tao, B. Panilaitis, M. Li, Z. Kang, F. Omenetto, Y. Huang and J. A. Rogers, *Small*, 2012, **8**, 3263–3268.
30 D. Kim, H.-C. Lee, J. Y. Woo and C.-S. Han, *J. Phys. Chem. C*, 2010, **114**, 5817–5821.
31 Y. H. Yoon, J. W. Song, D. Kim, J. Kim, J. K. Park, S. K. Oh and C. S. Han, *Adv. Mater.*, 2007, **19**, 4284–4287.
32 D. Sui, Y. Huang, L. Huang, J. Liang, Y. Ma and Y. Chen, *Small*, 2011, **7**, 3186–3192.
33 L. Liu, S. Peng, X. Niu and W. Wen, *Appl. Phys. Lett.*, 2006, **89**, 223521.
34 J. Kim, M. Lee, H. J. Shim, R. Ghaffari, H. R. Cho, D. Son, Y. H. Jung, M. Soh, C. Choi, S. Jung, K. Chu, D. Jeon, S.-T. Lee, J. H. K. Choi, S. Hong, T. Hyeo and D.-H. Kim, *Nat. Commun.*, 2014, **5**, 5747.
35 S. Choi, J. Park, W. Hyun, J. Kim, J. Kim, Y. B. Lee, C. Song, H. J. Hwang, J. H. Kim, T. Hyeon and D.-H. Kim, *ACS Nano*, 2015, **9**, 6626–6633.
36 S. Yao and Y. Zhu, *Adv. Mater.*, 2015, **27**, 1480–1511.
37 S. Hong, H. Lee, J. Lee, J. Kwon, S. Han, Y. D. Suh, H. Cho, J. Shin, J. Yeo and S. H. Ko, *Adv. Mater.*, 2015, **27**, 4744–4751.
38 C. Celle, C. Mayousse, E. Moreau, H. Basti, A. Carella and J.-P. Simonato, *Nano Res.*, 2012, **5**, 427–433.
39 F. Xu and Y. Zhu, *Adv. Mater.*, 2012, **24**, 5117–5122.
40 L. Song, A. C. Myers, J. J. Adams and Y. Zhu, *ACS Appl. Mater. Interfaces*, 2014, **6**, 4248–4253.
41 S. Yao and Y. Zhu, *Nanoscale*, 2014, **6**, 2345–2352.
42 D. Jung, M. Han and G. S. Lee, *J. Vac. Sci. Technol., B*, 2014, **32**, 04E105.
43 T. Kim, Y. W. Kim, H. S. Lee, H. Kim, W. S. Yang and K. S. Suh, *Adv. Funct. Mater.*, 2013, **23**, 1250–1255.
44 S. Wang, X. Zhang and W. Zhao, *J. Nanomater.*, 2013, **2013**, 3.

45 J. Kang, H. Kim, K. S. Kim, S.-K. Lee, S. Bae, J.-H. Ahn, Y.-J. Kim, J.-B. Choi and B. H. Hong, *Nano Lett.*, 2011, **11**, 5154–5158.
46 D. Kim, L. Zhu, D.-J. Jeong, K. Chun, Y.-Y. Bang, S.-R. Kim, J.-H. Kim and S.-K. Oh, *Carbon*, 2013, **63**, 530–536.
47 J. Li, J. Liang, X. Jian, W. Hu, J. Li and Q. Pei, *Macromol. Mater. Eng.*, 2014, **299**, 1403–1409.
48 T. J. Kang, T. Kim, S. M. Seo, Y. J. Park and Y. H. Kim, *Carbon*, 2011, **49**, 1087–1093.
49 S. Yun, X. Niu, Z. Yu, W. Hu, P. Brochu and Q. Pei, *Adv. Mater.*, 2012, **24**, 1321–1327.
50 J. Lee, P. Lee, H. Lee, D. Lee, S. S. Lee and S. H. Ko, *Nanoscale*, 2012, **4**, 6408–6414.
51 I. Blech and C. Herring, *Appl. Phys. Lett.*, 1976, **29**, 131–133.
52 M. Kaspers, A. Bernhart, F. M. zu Heringdorf, G. Dumpich and R. Möller, *J. Phys.: Condens. Matter*, 2009, **21**, 265601.
53 B. Stahlmecke, F.-J. M. zu Heringdorf, L. Chelaru, M. Horn-von Hoegen, G. Dumpich and K. Roos, *Appl. Phys. Lett.*, 2006, **88**, 053122.
54 T.-B. Song, Y. Chen, C.-H. Chung, Y. Yang, B. Bob, H.-S. Duan, G. Li, K.-N. Tu, Y. Huang and Y. Yang, *ACS Nano*, 2014, **8**, 2804–2811.
55 H. Oh, J. Lee, J.-H. Kim, J.-W. Park and M. Lee, *J. Phys. Chem. C*, 2016, **120**, 20471–20477.
56 D. Langley, M. Lagrange, G. Giusti, C. Jimenez, Y. Bréchet, N. D. Nguyen and D. Bellet, *Nanoscale*, 2014, **6**, 13535–13543.
57 S. Shian, K. Bertoldi and D. R. Clarke, *Adv. Mater.*, 2015, **27**, 6814–6819.
58 G. Fantoni, M. Santochi, G. Dini, K. Tracht, B. Scholz-Reiter, J. Fleischer, T. K. Lien, G. Seliger, G. Reinhart, J. Franke, H. N. Hansen and V. Alexander, *CIRP Ann. – Manuf. Technol.*, 2014, **63**, 679–701.
59 Y. Osada, H. Okuzaki and H. Hori, *Nature*, 1992, **355**, 242–244.
60 C. Yang, W. Wang, C. Yao, R. Xie, X.-J. Ju, Z. Liu and L.-Y. Chu, *Sci. Rep.*, 2015, **5**, 13622.
61 S. Maeda, Y. Hara, T. Sakai, R. Yoshida and S. Hashimoto, *Adv. Mater.*, 2007, **19**, 3480–3484.
62 C. Wu, J. Feng, L. Peng, Y. Ni, H. Liang, L. He and Y. Xie, *J. Mater. Chem.*, 2011, **21**, 18584–18591.
63 W.-H. Chu, M. Mehregany and R. L. Mullen, *J. Micromech. Microeng.*, 1993, **3**, 4–7.
64 N.-T. Nguyen and S. T. Wereley, *Fundamentals and applications of microfluidics*, Artech House, Boston, 2002.
65 J. A. Rogers, T. Someya and Y. Huang, *Science*, 2010, **327**, 1603–1607.
66 C. Bartholome, A. Derré, O. Roubeau, C. Zakri and P. Poulin, *Nanotechnology*, 2008, **19**, 325501.
67 X. Zhang, Z. Yu, C. Wang, D. Zarrouk, J.-W. T. Seo, J. C. Cheng, A. D. Buchan, K. Takei, Y. Zhao, J. W. Ager, J. Zhang, M. Hettick, M. C. Hersam, A. P. Pisano, R. S. Fearing and A. Javey, *Nat. Commun.*, 2014, **5**, 1–8.
68 Y. Jiang, C. Hu, H. Cheng, C. Li, T. Xu, Y. Zhao, H. Shao and L. Qu, *ACS Nano*, 2016, **10**, 4735–4741.